

A Group-Based Image Inpainting Using Patch Refinement in MRF Framework

Mrinmoy Ghorai^{ID}, Sekhar Mandal, and Bhabatosh Chanda

Abstract—This paper presents a Markov random field (MRF)-based image inpainting algorithm using *patch selection* from groups of similar patches and optimal *patch assignment* through joint *patch refinement*. In patch selection, a novel group formation strategy based on subspace clustering is introduced to search the candidate patches in relevant source region only. This improves patch searching in terms of both quality and time. We also propose an efficient patch refinement scheme using higher order singular value decomposition to capture underlying pattern among the candidate patches. This eliminates random variation and unwanted artifacts as well. Finally, a weight term is computed, based on the refined patches and is incorporated in the objective function of the MRF model to improve the optimal patch assignment. Experimental results on a large number of natural images and comparison with well-known existing methods demonstrate the efficacy and superiority of the proposed method.

Index Terms—Inpainting, subspace clustering, higher order singular value decomposition, Markov random field.

I. INTRODUCTION

IMAGE inpainting techniques generate visual information in the target region (also called unknown or missing region) of an image so that the inpainted image becomes visually pleasant. Two major applications of image inpainting techniques are image restoration (e.g., scratch and blob removal from old photograph) and image editing (e.g., text or undesired object removal). These methods may be broadly classified into two categories: (i) diffusion-based methods for structure propagation, and (ii) exemplar-based methods for texture synthesis.

In diffusion-based methods [1]–[4] information is smoothly propagated inward the missing region from its boundary. These methods use partial differential equation (PDE) to propagate linear structures along the *isophote* direction. PDE based methods are efficient for mostly thin target region (e.g., scratch) surrounded by smooth region. On the other hand, for the texture images, these methods may create a blurring effect due to the smoothing term.

Manuscript received April 20, 2017; revised August 4, 2017; accepted October 14, 2017. Date of publication October 30, 2017; date of current version November 9, 2017. This work was supported by the Department of Science and Technology, Government of India under Grant NRDMS/11/1586/09/Phase-I/Project No. 9. The associate editor coordinating the review of this manuscript and approving it for publication was Dr. Alin M. Achim. (*Corresponding author:* Mrinmoy Ghorai.)

M. Ghorai and B. Chanda are with the Electronics and Communication Sciences Unit, Indian Statistical Institute, Kolkata 700108, India.

S. Mandal is with the Indian Institute of Engineering Science and Technology, Shibpur, Howrah 711103, India.

Color versions of one or more of the figures in this paper are available online at <http://ieeexplore.ieee.org>.

Digital Object Identifier 10.1109/TIP.2017.2768180

The basic idea of exemplar- or patch-based methods is to fill the target region by copying the well-matched source patches (i.e., candidate patches from the source region) to the corresponding target locations. Initially, this idea was employed for texture synthesis [5], [6] for super resolution imaging. Later, Criminisi *et al.* [7] combined this approach with patch *priority* to devise an exemplar-based image inpainting method, where structure propagation is ensured by choosing the target patch lying on the structure for filling up first based on priority value. This work is further improved in [8]–[10] by modifying patch priority and patch similarity measures. Compared to diffusion-based approach, exemplar-based methods usually produce visually better result for blob type target region. These methods are greedy in nature as the target patches are inferred sequentially. So the error in patch inference at any stage is propagated till end. Komodakis *et al.* [11] solve this problem with MRF-based global optimization method which assigns an optimal patch to each node simultaneously from multiple candidate patches depending on the node's *belief*. A node's belief is determined based on the target patches assigned to its neighboring nodes, and the method is known as *priority belief propagation* (p-BP). Recently, *context-aware* patch-based image inpainting is introduced by Ruzic *et al.* [12], where candidate patches are searched over the entire source region based on contextual similarity. Meur *et al.* [13] propose super-resolution inpainting, where inpainted target region at different scales are combined in the lower scale using MRF-based framework. Then this lower resolution inpainted image is upsampled using single frame super-resolution technique to obtain inpainted image at the same scale as the input. Furthermore, He and Sun [14] solved image inpainting as a *photomontage* problem utilizing the statistics of patch offsets in MRF-based framework. This method is useful for the images having repeated objects.

Besides MRF-based methods, sparse representation is also widely used in image inpainting [15]–[18], where the target patch is inferred by sparse linear combination of a set of pre-defined patches (dictionary) or selected candidate patches. Usually searching candidate patches is a time intensive process. A fast randomized patch search algorithm called PatchMatch [19] is developed by exploiting natural coherence in the image using nearest neighbor field (NNF). Later, Darabi *et al.* [20] have proposed *image melding* to improve PatchMatch by incorporating geometric and photometric transformations in patch inference. In [14], patch offsets are found only in the image plane, whereas planar structure based method [21] finds the patch offsets in different

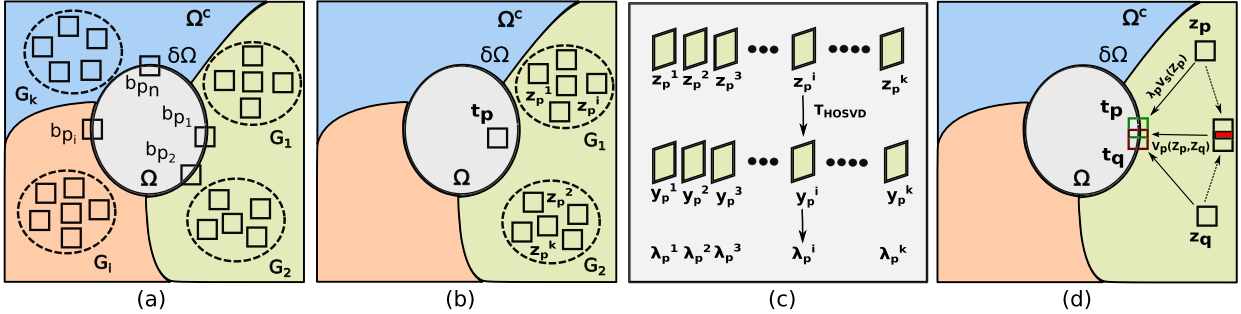


Fig. 1. An illustration of the proposed group-based image inpainting method using patch refinement in MRF framework. (a) Group formation: G_1, G_2, \dots, G_K are the groups formed by the candidates of the boundary patches $\{b_{p_1}, b_{p_2}, \dots, b_{p_n}\}$ where $K \leq n$. (b) Patch selection: For the target patch t_p , the groups G_1, G_2 are chosen and the candidate patches $\{z_p^1, z_p^2, \dots, z_p^k\}$ are selected from these groups. (c) Patch refinement: The patches $\{z_p^1, z_p^2, \dots, z_p^k\}$ are jointly filtered to obtain the refined patches $\{y_p^1, y_p^2, \dots, y_p^k\}$. (d) Modified MRF Optimization: $\lambda_p V_s(z_p)$ and $V_p(z_p, z_q)$ denote the single node potential and pairwise potential respectively, where the weight term λ_p is computed by the distance between z_p and y_p .

planes depending on translation regularity. This type of method is very useful for the architecture and indoor scene images where different planes may be found. Bugeau *et al.* [22] have proposed a comprehensive framework that combines three methods, namely diffusion [1], texture synthesis [5] and coherence [19], [23]. Pritch *et al.* [24] have assumed the fact that two neighboring patches in the target region should be similar to some pair of neighboring patches in the source region to facilitate patch searching. Further, a multiscale *graph cuts* algorithm [25] is used to solve image inpainting as a global energy optimization problem. Recently, Kumar *et al.* [26] have formulated image inpainting as a metric labeling problem and solved it using simulated annealing.

In this paper, our main contributions are (i) a group-based patch selection method to find the candidate patches from a restricted and proper search space, (ii) an efficient patch refinement method based on joint filtering of multiple patches to capture their underlying pattern by removing artifacts, and (iii) a modified objective function for the MRF model to improve the optimal patch assignment.

Most of the previous exemplar-based methods use either the entire source region [11]–[14] or some neighborhood of the target patch [18], [25] as search space. Though these methods produce acceptable results for many samples, they have some limitations. For example, patch ambiguity may arise if searching is performed in different segments of the source region. On the other hand, global consistency may not be preserved if the candidate patches are chosen from only a neighborhood. To overcome it, for each target patch we determine a relevant search space based on some pre-defined groups of patches and select the candidate patches only from this search space. As our first contribution, we propose a novel grouping method based on the candidates of the boundary patches (i.e. patches on the boundary of target region) using subspace clustering [27], [28] (shown in Fig. 1(a)). Thus the proposed method determines a reduced as well as suitable search space (shown in Fig. 1(b)) for patch selection and hence improves the quality of the inpainted image and time efficiency of the system.

Our second contribution is patch refinement, where the candidate patches are filtered jointly to capture their

underlying pattern and to remove artifacts. In exemplar-based methods [11]–[13], [17], [29], only a part of the candidate patch is used in the similarity measure which corresponds to the known region of the target patch. As a result, some incorrect patterns (e.g., artifacts) may be created in the inpainted region. To avoid it, we find the core pattern among the patches by jointly filtering them using higher order singular value decomposition (HOSVD) [30] (see Fig. 1(c)). Joint filtering of candidate patches was already suggested in image denoising [31], [32]. But, in this paper we adopt it for different purpose.

As a third contribution, a weight term is computed for each candidate patch depending on its refined version and this weight term is incorporated in the objective function of the MRF model (see Fig. 1(d)). This serves two main purposes: (i) improve optimal patch assignment in the patch inference step, and (ii) solve the problem of blurring effect introduced due to joint filtering. Therefore, instead of filtered patches, the original patches are assigned to the MRF nodes. In this work, the MRF-based optimization problem is solved by priority belief propagation (p-BP) [11].

Some part of this work (specifically joint filtering) was already presented in a conference [33]. Here we elaborate the idea with more analysis which improves the quality of the inpainted image. Rest of the paper is organized as follows. The main steps of the proposed method: group-based patch selection, patch refinement, and modified MRF optimization are presented in Section III. In Section IV, experimental results and comparisons with state-of-the-art methods are discussed. The paper is concluded in Section V. As our method is based on MRF model, in the next section (Section II), we briefly describe MRF framework for image inpainting.

II. MRF-BASED INPAINTING ALGORITHM

The MRF model can be represented by a graph $G = (\zeta, \varepsilon)$, where ζ and ε denote a set of nodes and a set of edges of the lattice, respectively. The nodes ζ consist of target patches in the unknown region Ω and the edges ε connect the patches in 4-neighborhood \mathcal{N}_4 on square lattice. The objective of MRF-based image inpainting is to assign an optimal label (patch) $z_p \in \mathcal{L}_p$ (a set of candidate patches) to each

target patch t_p at node $p \in \zeta$ in such a way that the following energy function \mathcal{E} is minimized.

$$\mathcal{E}(z) = \sum_{p \in \zeta} V_s(z_p) + \sum_{(p,q) \in \mathcal{N}_4} V_p(z_p, z_q) \quad (1)$$

where $V_s(z_p)$ and $V_p(z_p, z_q)$ denote the single node potential and pairwise potential respectively.

The single node potential $V_s(z_p)$ (also called *data term*) represents the cost of placing z_p at node p defined as

$$V_s(z_p) = \sum_{s \in W} \mathcal{M}(s)(t_p(s) - z_p(s))^2 \quad (2)$$

where W is window of size $h \times w$. $\mathcal{M}(\cdot)$ denotes a binary mask, which is 1 inside $\Omega^c \cap t_p$ and 0 otherwise. The pairwise potential cost $V_p(z_p, z_q)$ (also called *smoothness term*) represents the cost of placing the patches z_p and z_q at the 4-neighbors p and q respectively, and is given by

$$V_p(z_p, z_q) = \sum_{s \in W'} (z_p(u+s) - z_q(v+s))^2 \quad (3)$$

where W' is the overlapped region of z_p and z_q , and u, v indicate the overlapping offsets between the patches z_p and z_q .

III. PROPOSED INPAINTING METHOD

The proposed image inpainting method consists of three major steps: (i) group-based patch selection, (ii) HOSVD-based patch refinement, and (iii) modified MRF optimization. These steps are discussed in the following subsections.

A. Group-Based Patch Selection

In this paper, candidate patches are selected from a proper search space obtained from a set of groups of patches. The desired groups are constructed by merging a few subgroups, which are, in turn, the collection of source patches provided by the boundary patches. The advantage is that many improper source patches can be discarded from the search space, leading to a more reliable patch selection.

1) *Subgroup Computation*: Most of the exemplar-based methods [7], [9], [10], [17], [18] infer the target patches in sequential order from the boundary to the interior of the target region. Thus the interior patches depend on the boundary patches. We may argue that the candidates of the interior patches should be found within a neighborhood of the candidates of the boundary patches. So, all the source patches which are similar to a particular boundary patch, are considered to form a subgroup.

Let Z_p be a collection or subgroup of source patches similar to the boundary patch b_p located at $p \in \delta\Omega$. Z_p 's may be merged to form a larger collection called group. Similarity between the known part of the patch b_p and the corresponding part of the source patch $z_p \in \Omega^c$ is measured by sum of squared differences (SSD) defined as

$$Z_p = \left\{ z_p \in \Omega^c : d_{SSD}(b_p, z_p) < \epsilon \right\} \quad (4)$$

where

$$d_{SSD}(b_p, z_p) = \sum_{s \in b_p \cap \Omega^c} (b_p(s) - z_p(s))^2$$

and ϵ is the error tolerance parameter. A small ϵ prevents from selecting a source patch that is too different from the boundary patch. Another advantage of Eq. (4) is that it controls the size of the subgroups.

Let $X = \bigcup_{i=1}^n Z_{p_i}$ be the collection of all selected source patches, where n is the number of boundary patches or number of subgroups. Alternatively, X may be represented by $\{\mathbf{x}_j \in \mathbb{R}^d\}_{j=1}^N$, where N is the total number of selected patches and $d = h \times w \times 3$ is the dimension of a color patch. We divide X into K ($K \ll N$) groups $\mathcal{G} = [G_1, G_2, \dots, G_K]$ using subspace clustering. To achieve this, instead of applying a clustering algorithm directly on X , similar subgroups in $Z = [Z_{p_1}, Z_{p_2}, \dots, Z_{p_n}]$ are merged. This ensures all member patches of Z_{p_i} to be included into a single group G_j .

2) *Subspace Clustering and Group Formation*: Subspace clustering determines K subspaces $\{S_i\}_{i=1}^K$ (fitted over K groups) of unknown dimensions d_i where $0 < d_i < d$. The subspace S_i can be expressed as

$$S_i = \{\mathbf{x} \in \mathbb{R}^d : \mathbf{x} = \mathbf{m}_i + U_i \mathbf{y}\} \quad (5)$$

where $\mathbf{m}_i \in \mathbb{R}^d$ is an arbitrary point in subspace S_i , and $U_i \in \mathbb{R}^{d \times d_i}$ constitutes its basis. The point \mathbf{x} is represented by a low-dimensional point $\mathbf{y} \in \mathbb{R}^{d_i}$. Here, our main purpose of subspace clustering is to find the partition of patches into the subspaces. The motivation comes from the observation that two boundary patches that belong to same texture region have common similar patches. Therefore, similar subgroups are expected to lie in the same subspace and should be merged. In literature, several solutions are proposed for subspace clustering such as K-means projective clustering [34], spectral clustering [27], discriminative subspace clustering [28], sparse subspace clustering (SSC) [35]. It is used in a variety of computer vision problems like motion segmentation [36], face clustering [37] and image representation [38].

Let $S_{p_1}, S_{p_2}, \dots, S_{p_n}$ be the subspaces fitted over the subgroups $Z_{p_1}, Z_{p_2}, \dots, Z_{p_n}$ using principal component analysis (PCA). Distance between two subgroups Z_{p_u} and Z_{p_v} for $p_u, p_v \in \delta\Omega$, the boundary of the target region, is computed by [28]

$$D(Z_{p_u}, Z_{p_v}) = \frac{1}{2} \left(\sqrt{\xi(z_{p_v}, S_{p_u})} + \sqrt{\xi(z_{p_u}, S_{p_v})} \right) \quad (6)$$

where $\xi(z_{p_v}, S_{p_u})$ denotes the mean squared orthogonal distances of points $z_{p_v} \in Z_{p_v}$ to the subspace S_{p_u} estimated by Z_{p_u} and may be defined as

$$\xi(z_{p_v}, S_{p_u}) = \|z_{p_v} - \sum_{i=1}^{d_{p_u}} \langle z_{p_v}, e_i \rangle e_i\| \quad (7)$$

where d_{p_u} is the dimension of the subspace S_{p_u} , $\{e_1, e_2, \dots, e_{d_{p_u}}\}$ is the orthogonal basis of S_{p_u} , and $\langle z_{p_v}, e_i \rangle$ denotes the inner product between the vectors z_{p_v} and e_i . Thus, for each subgroup we first fit a subspace and then project the points of the other subgroup to that

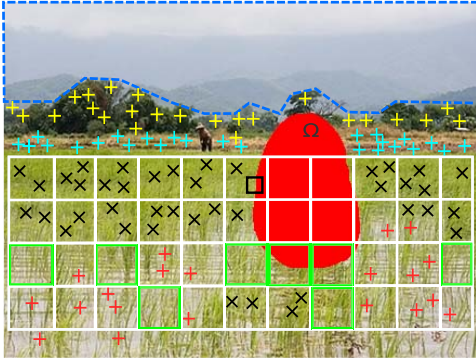


Fig. 2. An illustration of determining search space for the candidate patches. The patches marked by “+” and “x” symbols with different colors represent the patches of four different groups. For the target patch shown in black square, “x” are the locations of the patches of the selected group. The white blocks that contain “x” constitute the search space.

subspace. The distance ξ is a projection affinity based on the projection of high dimensional vectors to lower dimensional space [28], [39]. Typical distance based affinity matrix has a drawback that two points, which are very close to each other, may lie in different subspaces (e.g., points near the intersection of two subspaces). So, based on distance D , a projection affinity may be defined as geometric residual given by

$$\mathcal{H}(u, v) = \exp\{-D(Z_{p_u}, Z_{p_v})/\alpha\} \quad (8)$$

where α is a scaling parameter and it is set experimentally to 0.01. Now, spectral clustering [27] is applied on the eigen vectors of the normalized affinity matrix $\bar{\mathcal{H}}$, and the subgroups within a cluster are merged to yield the final groups $\mathcal{G} = [G_1, G_2, \dots, G_K]$. The number of groups is determined by the maximum difference between consecutive eigen values [27], and the intrinsic dimension of the subspaces is set to $d' = \max(d_{p_i})$ where d_{p_i} is the actual dimension of the subspace S_{p_i} fitted over the subgroup Z_{p_i} .

Fig. 2 shows that some regions of input image may not be considered in group formation because none of the boundary patches is similar to those regions, e.g., the “sky” and “hill” regions marked by dashed lines as well as the green blocks in the “field” region. Thus, the search space is reduced by discarding those irrelevant regions. Note that whether a region is relevant or not depends on the threshold ϵ in Eq. (4).

3) Search Space Estimation and Patch Selection: In this step, a relevant part of the source region is demarcated as search space. The main idea is to find the groups which are eligible to be a part of search space for specific target patches. The eligibility criterion is given by a similarity measure between a target patch and the representative patch of each group, which may be the group mean, i.e., average of all patches in the group. Finally, the image blocks that cover the patches of the selected groups constitute the search space.

For group selection, we propose a dissimilarity measure \mathcal{D} between a target patch t_p and the group mean μ_j of the group $G_j \in \mathcal{G}$ defined as

$$\mathcal{D}(t_p, \mu_j) = d_{SSD}(t_p, \mu_j) \cdot d_H(t_p, \mu_j), \quad (9)$$

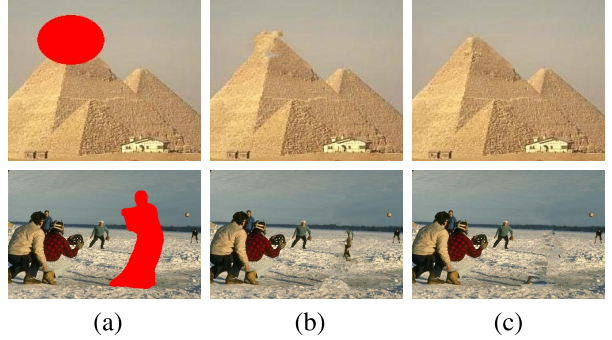


Fig. 3. (a) Target image with marked region. (b) Image inpainted by d_{SSD} . (c) Image inpainted by \mathcal{D} .

where the histogram-based distance $d_H(t_p, \mu_j)$ is given by

$$d_H(t_p, \mu_j) = -\log \sum_{i=1}^B \sqrt{H_{t_p}(i)H_{\mu_j}(i)}. \quad (10)$$

Here the histogram H_{t_p} is computed over only known pixels of the target patch t_p , and H_{μ_j} is the same but computed over the whole patch μ_j . B is the number of bins of the histogram. Since d_H is rotation invariant, we may still need SSD to distinguish the same patch in different orientations. Fig. 3 shows the inpainting results using dissimilarity measures \mathcal{D} and d_{SSD} for group selection. It is evident from the figure that dissimilarity measure \mathcal{D} produces better output.

Finally, a rectangle enveloping all the patches belonging to the selected groups is divided into non-overlapping blocks of size $h_b \times w_b$ as shown in Fig. 2. As such there is no relation between the block size and the patch size except that the former is larger than the latter. However, if the block size is too large, the number of improper candidate patches may increase which can make the process slow and worsen the quality of inpainted image. The block that contains at least one patch of the selected group is a part of the search space (e.g., white squares containing “x” in Fig. 2). During inpainting, the candidate patches are found only from the estimated search space based on the dissimilarity measure \mathcal{D} .

As discussed earlier, most of the exemplar-based methods choose either patches from the whole source region (i.e., global patches) [11]–[14] or patches from a neighborhood of the target patch (i.e., local patches) [18], [25]. However, the proposed approach select patches from a relevant part of the source region that may not be immediate neighborhood of the target patch. Fig. 4 shows that the proposed group-based patch selection improves the quality of the inpainted image compared to the global and local patch selection methods. In addition, our patch selection method is faster compared to global patch selection as patch search is performed in a reduced search space. The only overhead is the cost of group formation (once for inpainting an image) and group selection (for each target patch). In the next subsection, we introduce a patch refinement method to extract the underlying or core pattern of selected candidate patches and remove unwanted artifacts from them.

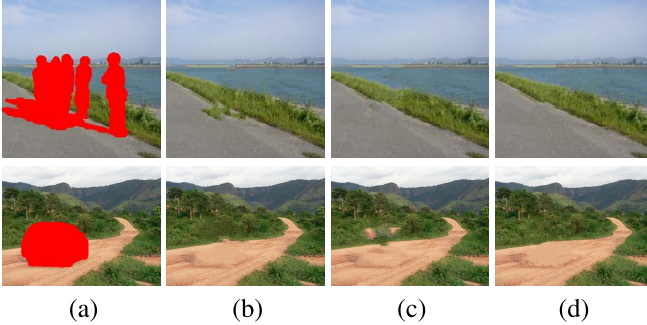


Fig. 4. (a) Target image with marked region. (b) Image inpainted by local patch selection. (c) Image inpainted by global patch selection. (d) Image inpainted by group-based patch selection.

B. HOSVD-Based Patch Refinement

Several exemplar-based methods use multiple patches in patch inference through weighted average [13], [29], sparse combination [15], [17] and MRF-based global optimization [11], [12]. These methods do not consider the variation in the patches which may play an important role in visual conformity. Since the candidate patches are chosen based on partially known target patch, a substantial variation may create artifacts in the inpainted region. To overcome it, a novel approach called patch refinement is proposed, where the selected candidate patches are filtered jointly to capture the core pattern amongst them which may help in finding an optimal patch for the corresponding target patch. Here joint filtering is realized through higher order singular value decomposition (HOSVD).

1) *Notations and Theory:* HOSVD is widely used to extract core information from multi-dimensional data due to its high performance and simple implementation. HOSVD has already been applied in image denoising [31], texture synthesis [40], super-resolution [41] and image fusion [42].

The HOSVD (also called Tensor-SVD) is an extension of the 2D matrix SVD to higher order matrix or tensor. Suppose $\mathcal{A} \in R^{n_1 \times n_2 \times \dots \times n_r}$ is a tensor of order r , where n_i denotes the number of elements in i -th dimension. The r-order tensor \mathcal{A} may be decomposed as follows [30]:

$$\mathcal{A} = \mathcal{S} \times_1 U^{(1)} \times_2 U^{(2)} \dots \times_r U^{(r)}, \quad (11)$$

where $U^{(1)}, U^{(2)}, \dots, U^{(r)}$ are the 2D orthogonal matrices computed from the SVD of the matrix unfolding $A_{(j)}$ with $j = 1, 2, \dots, r$, and \mathcal{S} is a coefficient array of size $n_1 \times n_2 \times \dots \times n_r$. Here, the symbol \times_s denotes the s-th mode tensor product defined in [30].

The core of tensor \mathcal{A} may be reconstructed by *hard thresholding* that ignores the singular values in the coefficient matrix \mathcal{S} below some pre-defined threshold. The concept of hard thresholding was employed in the wavelet reconstruction [43] and image denoising [31], [44]–[46] based on the assumption that the smaller coefficients are mostly dominated by noise. In image inpainting, hard thresholding may be applied to avoid artifacts (unwanted structure). Note that relatively larger coefficients may often appear due to artifacts in image patch. If we eliminate these coefficients by hard thresholding, fine information may also be removed producing smooth patch

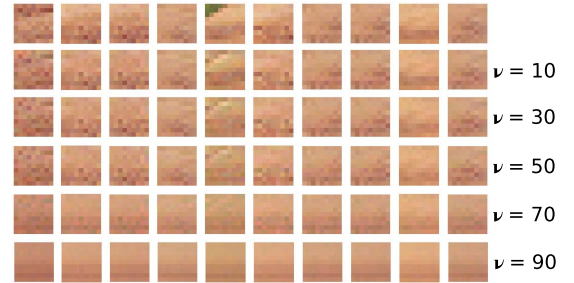


Fig. 5. The figure shows an example of joint filtering applied on a set of candidate patches shown in the first row. The remaining five rows show the refined patches for different values of v .

in fine texture area. To overcome this problem, we propose a new thresholding technique, namely *soft thresholding*, that nullifies a few larger coefficients representing the artifacts, and hence, preserves the texture clarity and image sharpness.

2) *Patch Refinement:* For a target patch t_p of size $w \times h$, we select k candidate patches by the method presented in Section III-A.3. These patches build a 3D stack to form a tensor $\mathcal{A} \in R^{w \times h \times k}$. The patch refinement consists of the following four steps:

- *Matricization:* Unfold the 3D tensor \mathcal{A} to the matrices $A_{(1)} \in R^{w \times hk}, A_{(2)} \in R^{h \times wk}$ and $A_{(3)} \in R^{k \times wh}$.
- *Decomposition:* Decompose $A_{(j)}$ using standard SVD to obtain orthogonal matrices $U^{(1)} \in R^{w \times w}, U^{(2)} \in R^{h \times h}, U^{(3)} \in R^{k \times k}$ and coefficient matrix $S_{(j)}$ for $j = 1, 2, 3$.
- *Nullification:* Nullify the coefficients which are between the lower threshold ($T_l = \sigma_1 \sqrt{2 \log(whk)}$) and the upper threshold ($T_u = \sigma_2 \sqrt{2 \log(whk)}$), where σ_1 and σ_2 are two parameters.
- *Inversion:* Reconstruct approximated tensor $\tilde{\mathcal{A}}$ by executing inversion of the transform.

In the above four steps, more crucial part is the selection of threshold parameters T_l and T_u . Tensor coefficients provide key information about the patches. Since candidate patches selected for a target patch are similar, most of the coefficients are either zero or very small and only a few are large. Though the larger coefficients carry the major information about the patches, some smaller coefficients may also have discriminating characteristics (due to fine texture) of the patches. Moreover, the largest coefficient captures the core pattern of the patches, while moderate coefficients usually represent high textural dissimilarity among the patches leading to artifacts. So the moderate coefficients need to be eliminated to remove the artifacts. The idea is similar to well known *band reject filter* [47] in digital signal processing.

To fix the threshold T_l , the value of σ_1 is chosen as the least coefficient whose frequency of occurrence in \mathcal{S} is less than a cut-off v . For the threshold T_u , instead of choosing a fixed value for σ_2 , the value of T_u is set to the second largest coefficient in \mathcal{S} . Fig. 5 shows an example of joint filtering using HOSVD. The first row shows the candidate patches where the fifth patch includes an artifact and the remaining rows show the refined patches for different values of v . The figure shows that the refined patches become smoother as the value of v increases, i.e., σ_1 decreases. However, desired

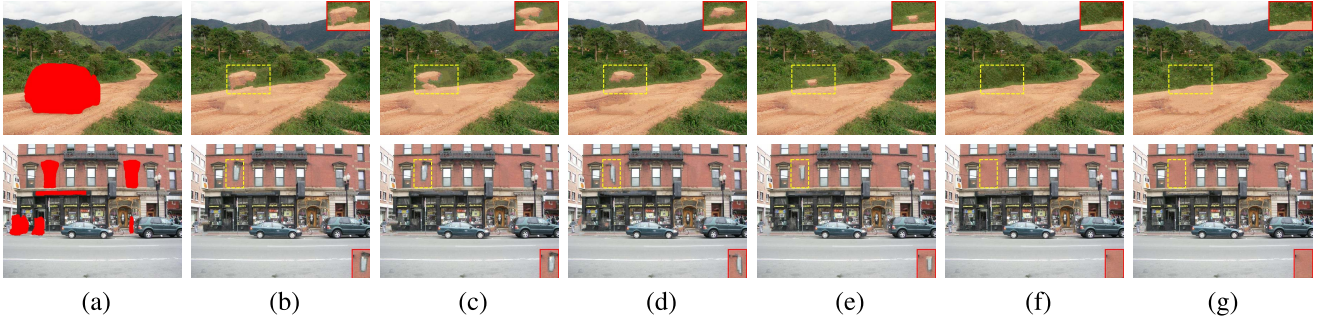


Fig. 6. Results due to different settings of σ_1 and σ_2 . (a) Target image with marked region. (b-g) Inpainted images for (b) $\sigma_1 = 0, \sigma_2 = 0.01$, (c) $\sigma_1 = 0, \sigma_2 = 0.1$, (d) $\sigma_1 = 0, \sigma_2 = 1$, (e) $\sigma_1 = 0, \sigma_2 = 10$, (f) $\sigma_1 = 0, \sigma_2 = 40$ and (g) $v = 30, T_u = \text{second largest coefficient}$.

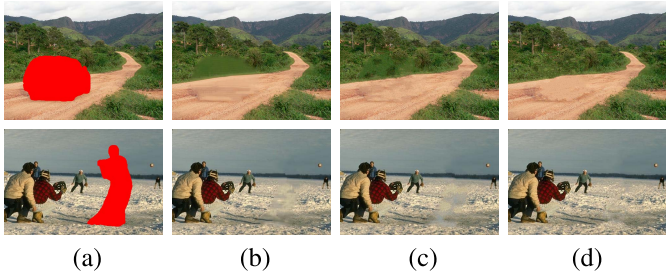


Fig. 7. (a) Target image with marked region. (b) Image inpainted by refined patches using hard thresholding. (c) Image inpainted by refined patches using soft thresholding. (d) Image inpainted by original patches.

result may be obtained for $v = 30$ where fine information is preserved and at the same time artifact is removed.

Fig. 6 illustrates the relationship between the coefficients in the core tensor and the artifacts. Fig. 6(b-f) show the inpainted images obtained by hard thresholding where $\sigma_1 = 0$ and σ_2 takes different values. As the value of σ_2 increases, larger coefficients (i.e., smaller frequencies) are nullified, and the artifacts are removed monotonically. This demonstrates our claim that artifacts may appear due to moderate values of the coefficients. However, the inpainted image (shown in Fig. 6(g)) obtained by the proposed soft thresholding technique looks usually better. Note that the value of σ_1 in the soft threshold changes with v which depends on the nature of the patches.

Fig. 7 shows that the patch refinement using soft thresholding improves texture sharpness of the inpainted region compared to hard thresholding. However, the proposed approach still has the problems of texture clarity and image sharpness in case of fine texture as it is hard to distinguish the coefficients representing the artifacts or the finer variation among the patches. To recover the texture quality, we propose a modified MRF model as described in the next subsection.

C. Modified MRF Optimization

The proposed MRF-based image inpainting framework minimizes the energy function (following Eq. (1)) given by

$$\mathcal{E}(z) = \sum_{p \in \zeta} \lambda_p V_s(z_p) + \sum_{(p,q) \in \mathcal{N}_4} V_p(z_p, z_q), \quad (12)$$

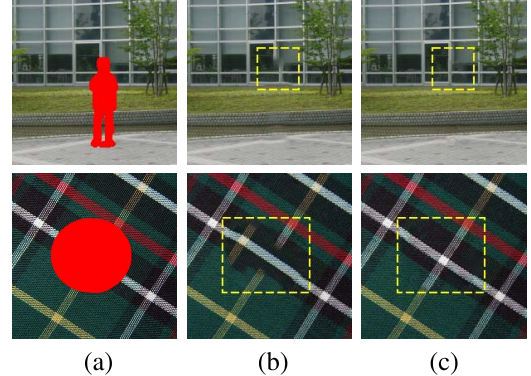


Fig. 8. Effect of λ . (a) Target image with marked region. (b) Image inpainted without λ (using Eq. (1)). (c) Image inpainted with λ (using Eq. (12) and Eq. (13)).

where λ_p is a measure of dissimilarity defined as

$$\lambda_p = \sum_{s \in W} (z_p(s) - y_p(s))^2, \quad (13)$$

where y_p is the refined patch as described in Section III-B.2. The term λ_p is a measure of dissimilarity between the candidate patch and the corresponding refined patch. If the candidate patch differs from the refined patch, the algorithm reduces the confidence value assigned to it. Thus the weight term λ facilitates the selection of optimal patch for the lattice nodes in MRF framework. Fig. 8 shows the effect of λ in image inpainting. It is clearly visible that the results (Fig. 8 (b)) due to traditional MRF (Eq. (1)) suffers from wrong patch assignment, which is rectified successfully by the proposed modified MRF (Eq. (12)) as shown in Fig. 8 (c).

Optimization of the energy function (Eq. (12)) may be done using loopy belief propagation (LBP) [48], [49] or priority belief propagation (p-BP) [11]. The key idea of these methods is belief propagation (BP), where local messages are continuously propagated between the nodes of an MRF lattice. However, LBP may not be appropriate for this work since a huge number messages need to be computed for the labels of the MRF nodes. In this work we have employed p-BP [11] where a specific priority message scheduling and label pruning (discarding improper patches) algorithms are introduced.

In BP, the message sent from node p to its neighboring node q is denoted by $\{m_{pq}(z_q)\}_{z_q \in \mathcal{L}}$ and is defined as

$$m_{pq}(z_q) = \min_{z_p \in \mathcal{L}} \left\{ \lambda_p V_s(z_p) + V_p(z_p, z_q) + \sum_{r:r \neq q, (r,p) \in \mathcal{N}_4} m_{rp}(z_p) \right\}. \quad (14)$$

Thus the message $m_{pq}(z_q)$ depends on the messages at node p received from its neighboring nodes other than q . Then beliefs $\{b_p(z_p)\}_{z_p \in \mathcal{L}}$ for every node p in the MRF is estimated as

$$b_p(z_p) = -\lambda_p V_s(z_p) - \sum_{r:(r,p) \in \mathcal{N}_4} m_{rp}(z_p). \quad (15)$$

Empirically, the belief $b_p(z_p)$ represents the probability of assigning label (i.e. patch) z_p to p , and it depends on the messages coming from the neighboring nodes of p . So a node is assigned the label having maximum belief

$$\hat{z}_p = \arg \max_{z_p \in \mathcal{L}} b_p(z_p). \quad (16)$$

In essence, the p-BP method consists of three steps: assigning node *priority*, *label pruning* and *inference*. The priority of an MRF node is determined by the number of eligible patches (in terms of belief) at that node, and usually lower the number, higher is the priority. In label pruning, the nodes are visited in the order of their priority. Then we select candidate patches using the method described in Section III-A.3, and discard rest of the patches. In inference, we employ priority scheduling message passing algorithm [11] in order to visit each MRF node and collect messages from its neighboring nodes for determining its belief. This process runs iteratively and updates the messages at each node until a convergence criterion is satisfied. The convergence criterion may be either the difference between two consecutive results becomes negligible or a fixed number of iterations is executed. According to Eq. (16), at each node the algorithm chooses the label that maximizes the node's belief. Then the patches are copied to the MRF nodes (in parallel) to generate the inpainted image. We incorporate pyramid-based approach (as in [11]) in our proposed method to preserve global consistency by multiscale feature representation. A pseudo-code of the proposed image inpainting method using p-BP is given in Algorithm 1.

IV. EXPERIMENTAL RESULTS AND DISCUSSION

In this section, we first set the parameters and then evaluate the proposed method through both quantitative and qualitative analysis on different types of inpainting problems such as scratch and blob/object removal. We compare our algorithm with the state-of-the-art methods such as Criminisi's exemplar [7],² Komodakis's p-BP [11],³ Pritch's shift-map [24], Darabi's image melding [20],⁴ Liu's graph cuts [25], Meur's super-resolution [13]⁵ and Ruzic's context-aware [12] based methods.

Algorithm 1 Proposed Image Inpainting Using p-BP

```

1: Form the groups  $\mathcal{G} = [G_1, G_2, \dots, G_K]$  as described in
   Section III-A1, A2
2: for  $i = 1$  to  $|\zeta|$  do  $\{\zeta\}$  is the total number of nodes}
3:   compute priority as defined in [11]
4:   set  $v_i = 0$   $\{v_i = 0$  if the node is unvisited or  $v_i = 1$ 
   if the node is visited}
5: end for
6: for  $i = 1$  to  $|\zeta|$  do
7:   Find the unvisited node  $p$  with highest priority.
8:   apply label pruning to node  $p$ : choose  $k$  patches  $z_p$ 
   (see Section III-A3) and discard the others from  $\mathcal{L}_p$ 
9:   compute  $\lambda_p$  using Eq. (13)
10:  for any neighbor  $q$  of  $p$  such that  $v_q = 0$  do
11:    send all messages  $m_{pq}(z_q)$  (Eq. (14))
12:    update beliefs  $b_p(z_p)$  (Eq. (15)) and priority of  $q$ 
13:  end for
14:  set  $v_p = 1$ 
15: end for
16:  $\hat{z}_p = \arg \max_{z_p \in \mathcal{L}} b_p(z_p)$  for every node  $p$ 

```

In our experiments, the patch size is set to $w = h = 9$, and ϵ is set to $100 \times |b_p \cap \Omega^c|$. We set the dimension of the subspaces to 8, and the size of the rectangular block as $h_b = w_b = 40$. In p-BP optimization, the maximum number of labels is $k = 30$ and the maximum number of iterations is 10. These parameters are selected through rigorous experimentation.

A. Qualitative and Quantitative Comparison for Scratch and Blob Removal

For quantitative evaluation we consider six images. Out of these images, long and thin scratches are created as unknown regions in three images (shown in top three rows of Fig. 9) and in the remaining three images blob type unknown regions are created (shown in the bottom three rows of Fig. 9). The images with marked target regions are shown in the second column. The proposed method is compared in terms of peak-signal-to-noise ratio (PSNR) with some of the well-known methods such as exemplar [7], p-BP [11], image melding [20], super-resolution [13] and context-aware [12] based methods. Here PSNR is computed only over the filled target region. It clearly shows that in most of the cases the proposed method recovers the missing information (scratch and blob) better, both quantitatively (w.r.t. PSNR) and qualitatively (by visual inspection) compared to other methods mentioned above except [20]. In some cases of scratch removal, image melding [20] performs slightly better than the proposed method.

B. Qualitative Comparison for Object Removal

We apply the proposed method to the blob type target region that occurs mostly in object removal and compare our method with some state-of-the-art inpainting methods. Here the task

²<http://www.cc.gatech.edu/~sooraj/inpainting/>

³<http://lafarren.com/image-completer/>

⁴<http://www.ece.ucsb.edu/~psen/melding/>

⁵http://people.irisa.fr/Olivier.Le_Meur/

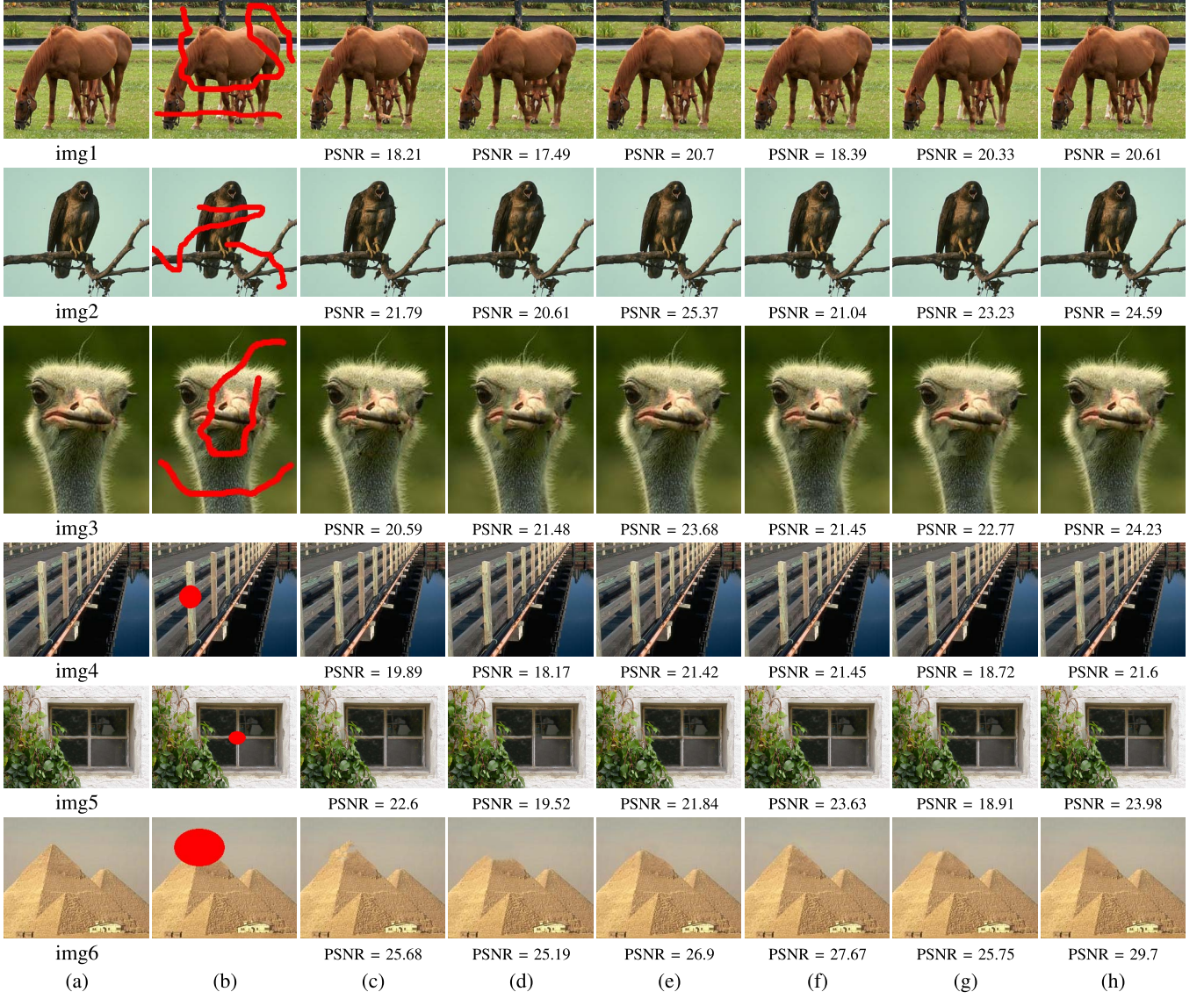


Fig. 9. Qualitative and quantitative comparison of different inpainting methods for scratch and blob removal. (a) Original image. (b) Damaged image. The inpainting results due to (c) exemplar-based [7], (d) p-BP [11], (e) image melding [20], (f) super-resolution [13], (g) context-aware [12], and (h) proposed method.

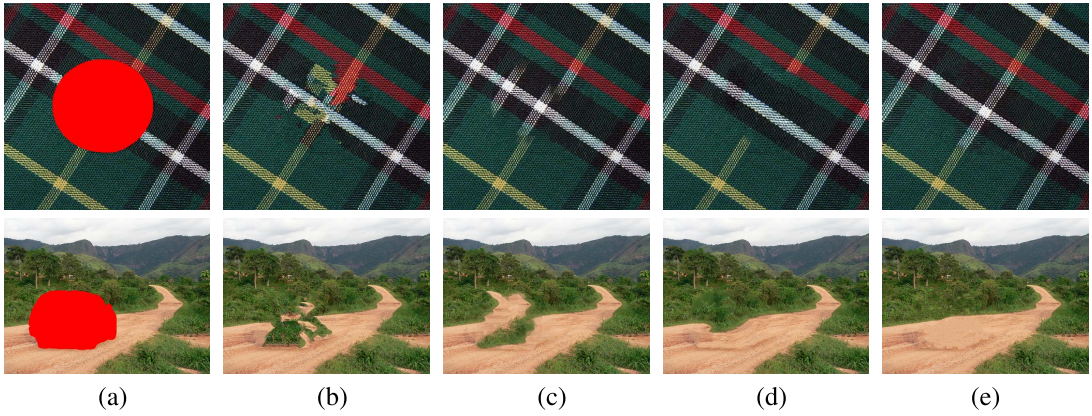


Fig. 10. (a) Target image with marked region. (b) Exemplar-based [7]. (c) p-BP [11]. (d) Image melding [20]. (e) Proposed method.

is relatively difficult as the target region is large and often surrounded by heterogeneous background.

The comparison between the proposed method and image melding [20] is shown in Fig. 10. The image melding method

incorporates photometric and geometric transformations in patch selection to exploit natural coherence in the image. This helps to improve exemplar-based method [7] (Fig. 10(b)) and p-BP method [11] (Fig. 10(c)) in case of texture synthesis.

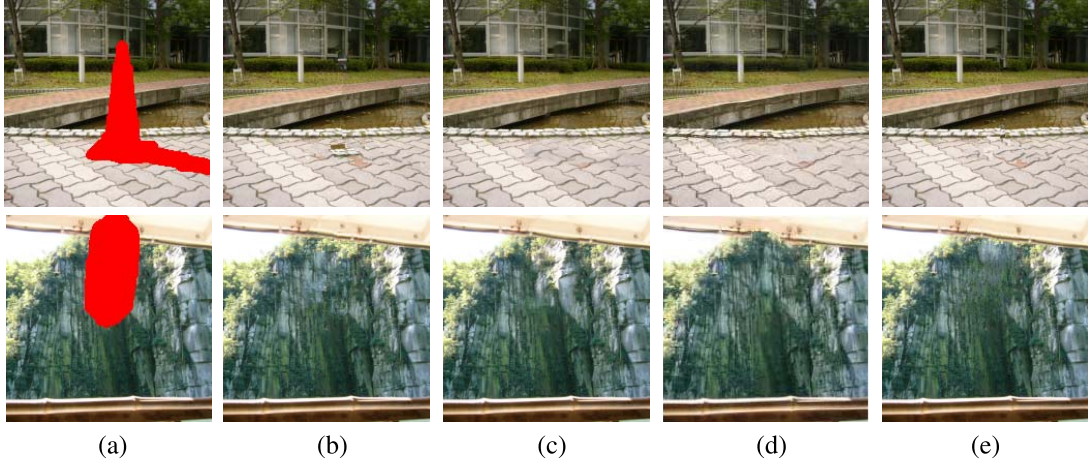


Fig. 11. (a) Target image with marked region. (b) Exemplar-based [7]. (c) p-BP [11]. (d) Graph cuts [25]. (e) Proposed method.



Fig. 12. (a) Target image with marked region. (b) Exemplar-based [7]. (c) p-BP [11]. (d) Super-resolution based [13]. (e) Proposed method.

However, sometimes image melding [20] fails to generate structure information as shown in Fig. 10(d). Our method recovers both texture and structure quite successfully (see Fig. 10(e)). Some explanation of good performance of our method is already illustrated in Figs. 4 and 8 with the first example of Fig. 10.

The examples shown in Fig. 11 are taken from the database <http://yokoya.naist.jp/research/inpainting/>. We carefully study the results of the proposed method and graph cuts [25] along with the methods [7] and [11]. Both the proposed method and graph cuts [25] use global optimization strategy. Moreover, due to proper patch selection and patch refinement our method produces better results than graph cuts [25] as well as [7] and [11] in terms of recovery of texture (e.g., “bricks” in the first example) and structure (e.g., lines in the second example).

The comparison with the single frame super-resolution based inpainting method [13] is shown in Fig. 12. This method combines multiple inpainted versions of the input image, which are obtained by different transformations such as scaling and rotation. However, the proposed method with proper patch selection and patch refinement produces significantly better results. For example, in case of top-left image, super-resolution based [13] as well as the methods proposed in [7] and [11] fail to maintain spatial coherence in the texture region, while the proposed method recovers the texture quite accurately. Moreover, the proposed method successfully removes artifacts in the second example.

Fig. 13 illustrates the superiority of the proposed method over another recent method based on context-aware MRF [12], where the structural context of image blocks is considered in patch selection. However, our group based patch selection and patch refinement jointly produces better results than [12] in terms of both structure completion (see the first row) and texture synthesis (see the second row).

Fig. 14 compares the result of the proposed method with sparsity-based [17] and multi-direction feature (MDF) [18]. The method [17] enforces local consistency constraint and patch sparsity using color feature, and further, MDF [18] improves it using a combined feature representation of color and direction. However, our method accumulates confidence from the neighboring nodes to assign optimal label to target node. As a result, it is found to be more effective than [17] and [18]. For example, sparsity-based [17] and MDF-based [18] methods fail to recover the structure consistency, whereas our method recovers those information quite successfully.

In Fig. 15, our method is compared with the method based on metric labeling [26] along with [11] and [13]. The method [26] combines multiple inpainted images obtained through different initialization using metric labeling. The figure shows that our method is able to reconstruct the structure (e.g., the line on the building in the first example) better compared to other methods. In case of texture recovery, the second example shows that the proposed method performs

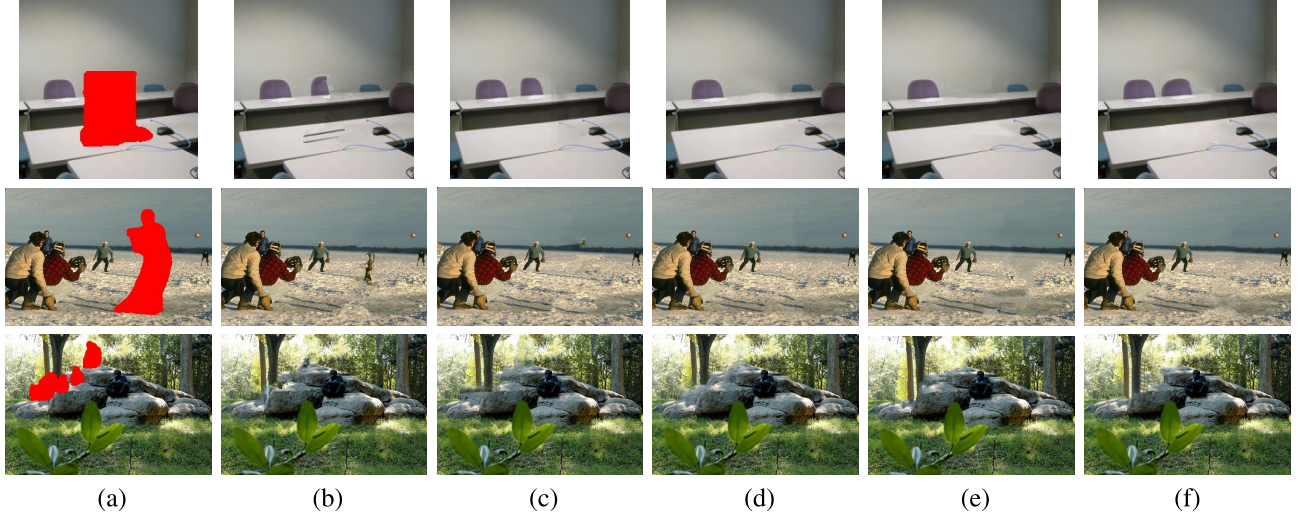


Fig. 13. (a) Target image with marked region. (b) Exemplar-based [7]. (c) p-BP [11]. (d) Image melding [20]. (e) Context-aware [12]. (f) Proposed method.

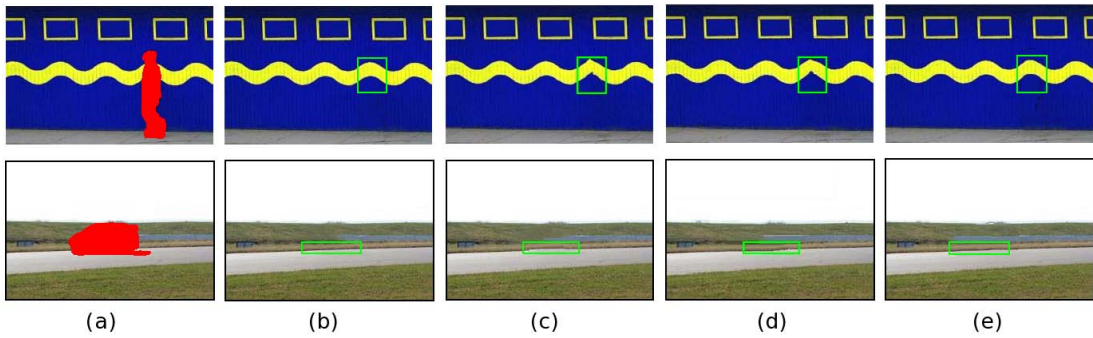


Fig. 14. (a) Target image with marked region. (b) p-BP [11]. (c) Sparsity-based [17]. (d) MDF [18]. (e) Proposed method.

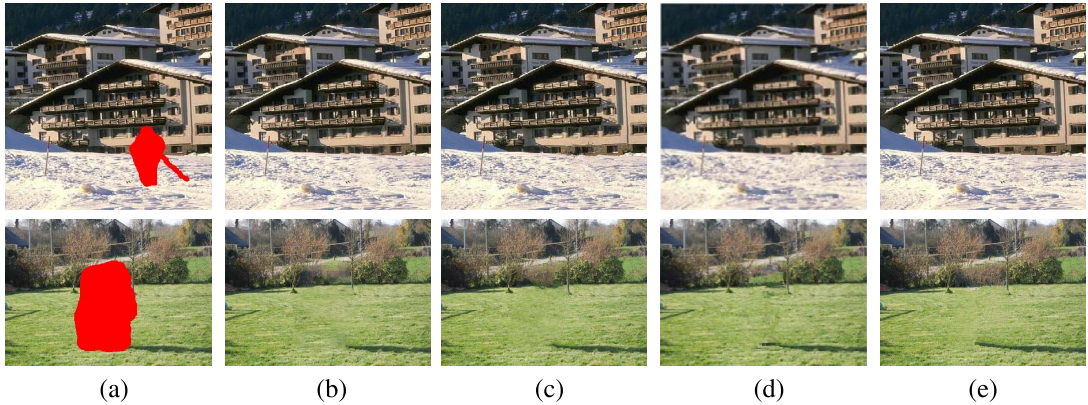


Fig. 15. (a) Target image with marked region. (b) p-BP [11]. (c) Super-resolution based [13]. (d) Metric labeling [26]. (e) Proposed method.

better than [11] (where a blur effect appears) and [26] (where an artifact appears on the tree); and is almost comparable to [13].

C. Some Failure Cases

In Fig. 16, we have shown some examples where the proposed method along with the competitive methods fail to recover proper texture in the target region. In the first example, texture of the curtain is not successfully generated due to illumination variation in the image. However, even

in most of the failure cases, our results are relatively less erroneous than the other approaches (see the second example). We observe that the proposed method may fail when the target region is surrounded by irregular texture, because, in that case, representing it in RGB feature space is difficult.

D. Comparison of Time Requirement

The proposed method is implemented using MATLAB on Intel 3.07 GHz CPU with 8GB RAM. The computation times of different methods are shown in TABLE I for the test images

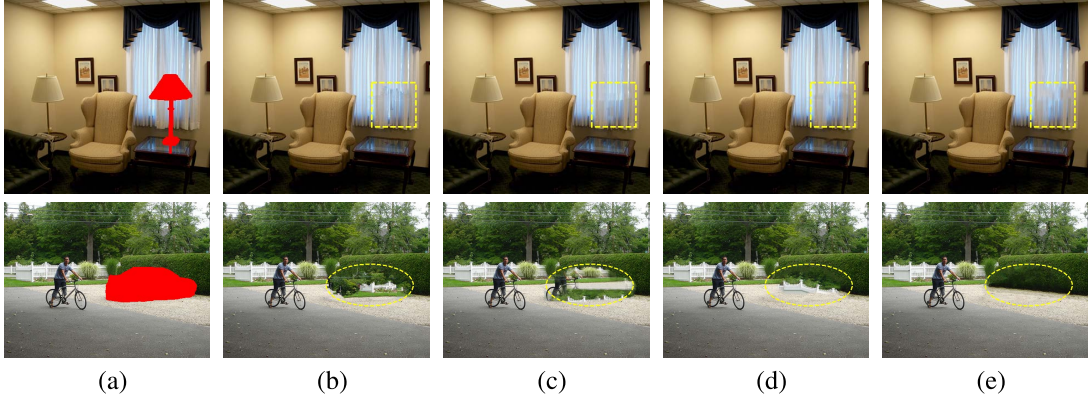


Fig. 16. Failure cases. (a) Target image with marked region. (b) Exemplar-based [7]. (c) p-BP [11]. (d) Image melding [20]. (e) Proposed method.

TABLE I
COMPUTATIONAL TIMES FOR DIFFERENT METHODS IN SECONDS

| Examples | Exemplar-based [7] | p-BP [11] | Image melding [20] | Context-aware [12] | Proposed method |
|------------|--------------------|-----------|--------------------|--------------------|-----------------|
| “office” | 6.23 | 214.23 | 821.21 | 58.42 | 62.74 |
| “baseball” | 70.57 | 1295.95 | 4048.17 | 499.50 | 584.70 |
| “gorilla” | 42.02 | 640.78 | 5048.48 | 251.87 | 297.50 |

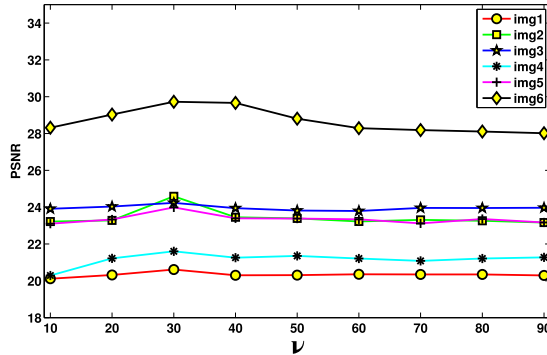


Fig. 17. Plots of PSNR versus v for the images taken from Fig. 9.

of Fig. 13. The proposed method is better in computation time and the quality of the results compared to p-BP [11] and image melding [20]. However, it is slightly slower than context-aware [12]. This is due to the fact that patch refinement takes significant time (approximately half) with respect to the whole process. But, our method produces better results in most of the cases compared to [12] as shown in Fig. 13.

E. Parameter Analysis

One of the important parameters in the proposed image inpainting method is v which is used in patch refinement. In Fig. 17, we have shown the plots of PSNR versus v for six images of Fig. 9 to demonstrate its effect in quality of inpainting. The figure shows that consistently good results may be obtained for $v = 30$. As the value of v increases more coefficients are nullified, and hence, a smoothing effect may appear in the inpainted region.

V. CONCLUSION

In this paper, we have proposed an MRF-based image inpainting method where candidate patches are chosen based

on some preformed groups of patches. Due to this group formation we can reduce search time for candidate patches and avoid selecting irrelevant patches. We have also introduced patch refinement based on joint filtering of the candidate patches to extract the core pattern. This helps in finding the optimal label for each MRF node. As a consequence, good results are produced, which is evident from the results shown on various natural images. In future, we plan to investigate different transformations in our method for more robust patch selection.

REFERENCES

- [1] M. Bertalmio, G. Sapiro, V. Caselles, and C. Ballester, “Image inpainting,” in *Proc. ACM SIGGRAPH Conf. Comput. Graph.*, 2000, pp. 417–424.
- [2] T. F. Chan and J. Shen, “Nontexture inpainting by curvature-driven diffusions,” *J. Vis. Commun. Image Represent.*, vol. 12, no. 4, pp. 436–449, 2001.
- [3] D. Tschumperlé, “Fast anisotropic smoothing of multi-valued images using curvature-preserving PDE’s,” *Int. J. Comput. Vis.*, vol. 68, no. 1, pp. 65–82, 2006.
- [4] F. Bornemann and T. März, “Fast image inpainting based on coherence transport,” *J. Math. Imag. Vis.*, vol. 28, no. 3, pp. 259–278, 2007.
- [5] A. A. Efros and T. K. Leung, “Texture synthesis by non-parametric sampling,” in *Proc. IEEE Int. Conf. Comput. Vis.*, vol. 2, Sep. 1999, pp. 1033–1038.
- [6] V. Kwatra, A. Schödl, I. Essa, G. Turk, and A. Bobick, “Graphcut textures: Image and video synthesis using graph cuts,” *ACM Trans. Graph.*, vol. 22, no. 3, pp. 277–286, 2003.
- [7] A. Criminisi, P. Perez, and K. Toyama, “Region filling and object removal by exemplar-based image inpainting,” *IEEE Trans. Image Process.*, vol. 13, no. 9, pp. 1200–1212, Sep. 2004.
- [8] J. Sun, L. Yuan, J. Jia, and H.-Y. Shum, “Image completion with structure propagation,” *ACM Trans. Graph.*, vol. 24, no. 3, pp. 861–868, 2005.
- [9] J. Wu and Q. Ruan, “Object removal by cross isophotes exemplar-based inpainting,” in *Proc. IEEE Int. Conf. Pattern Recognit.*, vol. 3, Aug. 2006, pp. 810–813.
- [10] Y. Qin and F. Wang, “A curvature constraint Exemplar-based image inpainting,” in *Proc. Int. Conf. Image Anal. Signal Process.*, Apr. 2010, pp. 263–267.

- [11] N. Komodakis and G. Tziritas, "Image completion using efficient belief propagation via priority scheduling and dynamic pruning," *IEEE Trans. Image Process.*, vol. 16, no. 11, pp. 2649–2661, Nov. 2007.
- [12] T. Ruzic and A. Pizurica, "Context-aware patch-based image inpainting using Markov random field modeling," *IEEE Trans. Image Process.*, vol. 24, no. 1, pp. 444–456, Jan. 2015.
- [13] O. Le Meur, M. Ebdelli, and C. Guillemot, "Hierarchical super-resolution-based inpainting," *IEEE Trans. Image Process.*, vol. 22, no. 10, pp. 3779–3790, Oct. 2013.
- [14] K. He and J. Sun, "Statistics of patch offsets for image completion," in *Proc. 12th Eur. Conf. Comput. Vis.*, 2012, pp. 16–29.
- [15] M. J. Fadili, J.-L. Starck, and F. Murtagh, "Inpainting and zooming using sparse representations," *Comput. J.*, vol. 52, no. 1, pp. 64–79, 2009.
- [16] B. Shen, W. Hu, Y. Zhang, and Y.-J. Zhang, "Image inpainting via sparse representation," in *Proc. IEEE Int. Conf. Acoust., Speech Signal Process.*, Apr. 2009, pp. 697–700.
- [17] Z. Xu and J. Sun, "Image inpainting by patch propagation using patch sparsity," *IEEE Trans. Image Process.*, vol. 19, no. 5, pp. 1153–1165, May 2010.
- [18] Z. Li, H. He, H. M. Tai, Z. Yin, and F. Chen, "Color-direction patch-sparsity-based image inpainting using multidirection features," *IEEE Trans. Image Process.*, vol. 24, no. 3, pp. 1138–1152, Mar. 2015.
- [19] C. Barnes, E. Shechtman, A. Finkelstein, and D. B. Goldman, "PatchMatch: A randomized correspondence algorithm for structural image editing," *ACM Trans. Graph.*, vol. 28, no. 3, pp. 1–10, 2009.
- [20] S. Darabi, E. Shechtman, C. Barnes, D. B. Goldman, and P. Sen, "Image melding: Combining inconsistent images using patch-based synthesis," *ACM Trans. Graph.*, vol. 31, no. 4, pp. 1–10, 2012.
- [21] J.-B. Huang, S. B. Kang, N. Ahuja, and J. Kopf, "Image completion using planar structure guidance," *ACM Trans. Graph.*, vol. 33, no. 4, 2014, Art. no. 129.
- [22] A. Bugeau, M. Bertalmio, V. Caselles, and G. Sapiro, "A comprehensive framework for image inpainting," *IEEE Trans. Image Process.*, vol. 19, no. 10, pp. 2634–2645, Oct. 2010.
- [23] Y. Wexler, E. Shechtman, and M. Irani, "Space-time completion of video," *IEEE Trans. Pattern Anal. Mach. Intell.*, vol. 29, no. 3, pp. 463–476, Mar. 2007.
- [24] Y. Pritch, E. Kav-Venaki, and S. Peleg, "Shift-map image editing," in *Proc. IEEE Int. Conf. Comput. Vis.*, Sep. 2009, pp. 151–158.
- [25] Y. Liu and V. Caselles, "Exemplar-based image inpainting using multiscale graph cuts," *IEEE Trans. Image Process.*, vol. 22, no. 5, pp. 1699–1711, May 2013.
- [26] V. Kumar, J. Mukherjee, and S. K. D. Mandal, "Image inpainting through metric labeling via guided patch mixing," *IEEE Trans. Image Process.*, vol. 25, no. 11, pp. 5212–5226, Nov. 2016.
- [27] A. Y. Ng, M. I. Jordan, and Y. Weiss, "On spectral clustering: Analysis and an algorithm," in *Proc. Adv. Neural Inf. Process. Syst.*, vol. 2. 2001, pp. 849–856.
- [28] V. Zografos, L. Ellis, and R. Mester, "Discriminative subspace clustering," in *Proc. IEEE Conf. Comput. Vis. Pattern Recognit. (CVPR)*, Jun. 2013, pp. 2107–2114.
- [29] A. Wong and J. Orchard, "A nonlocal-means approach to exemplar-based inpainting," in *Proc. IEEE Int. Conf. Image Process.*, Oct. 2008, pp. 2600–2603.
- [30] L. De Lathauwer, B. De Moor, and J. Vandewalle, "A multilinear singular value decomposition," *SIAM J. Matrix Anal. Appl.*, vol. 21, no. 4, pp. 1253–1278, 2000.
- [31] A. Rajwade, A. Rangarajan, and A. Banerjee, "Image denoising using the higher order singular value decomposition," *IEEE Trans. Pattern Anal. Mach. Intell.*, vol. 35, no. 4, pp. 849–862, Apr. 2013.
- [32] K. Dabov, A. Foi, V. Katkovnik, and K. Egiazarian, "Image denoising by sparse 3-D transform-domain collaborative filtering," *IEEE Trans. Image Process.*, vol. 16, no. 8, pp. 2080–2095, Aug. 2007.
- [33] M. Ghorai and B. Chanda, "An image inpainting algorithm using higher order singular value decomposition," in *Proc. ICPR*, Aug. 2014, pp. 2867–2872.
- [34] P. K. Agarwal and N. H. Mustafa, "K-means projective clustering," in *Proc. ACM SIGMOD-SIGACT-SIGART Symp. Principles Database Syst.*, 2004, pp. 155–165.
- [35] E. Elhamifar and R. Vidal, "Sparse subspace clustering," in *Proc. IEEE Conf. Comput. Vis. Pattern Recognit.*, Jun. 2009, pp. 2790–2797.
- [36] Z. Li, J. Guo, L.-F. Cheong, and S. Z. Zhou, "Perspective motion segmentation via collaborative clustering," in *Proc. IEEE Int. Conf. Comput. Vis. (ICCV)*, Dec. 2013, pp. 1369–1376.
- [37] A. Adler, M. Elad, and Y. Hel-Or, "Probabilistic subspace clustering via sparse representations," *IEEE Signal Process. Lett.*, vol. 20, no. 1, pp. 63–66, Jan. 2013.
- [38] W. Hong, J. Wright, K. Huang, and Y. Ma, "Multiscale hybrid linear models for lossy image representation," *IEEE Trans. Image Process.*, vol. 15, no. 12, pp. 3655–3671, Dec. 2006.
- [39] E. Bingham and H. Mannil, "Random projection in dimensionality reduction: Applications to image and text data," in *Proc. ACM SIGKDD Int. Conf. Knowl. Discovery Data Mining*, 2001, pp. 245–250.
- [40] R. Costantini, L. Sbaiz, and S. Susstrunk, "Higher order SVD analysis for dynamic texture synthesis," *IEEE Trans. Image Process.*, vol. 17, no. 1, pp. 42–52, Jan. 2008.
- [41] W. Liu, D. Lin, and X. Tang, "Hallucinating faces: TensorPatch super-resolution and coupled residue compensation," in *Proc. IEEE Conf. Comput. Vis. Pattern Recognit.*, vol. 2. Jun. 2005, pp. 478–484.
- [42] J. Liang, Y. He, D. Liu, and X. Zeng, "Image fusion using higher order singular value decomposition," *IEEE Trans. Image Process.*, vol. 21, no. 5, pp. 2898–2909, May 2012.
- [43] D. L. Donoho and J. M. Johnstone, "Ideal spatial adaptation by wavelet shrinkage," *Biometrika*, vol. 81, no. 3, pp. 425–455, 1994.
- [44] X. Zhang, W. Lin, R. Xiong, X. Liu, S. Ma, and W. Gao, "Low-rank decomposition-based restoration of compressed images via adaptive noise estimation," *IEEE Trans. Image Process.*, vol. 25, no. 9, pp. 4158–4171, Sep. 2016.
- [45] Q. Guo, C. Zhang, Y. Zhang, and H. Liu, "An efficient SVD-based method for image denoising," *IEEE Trans. Circuits Syst. Video Technol.*, vol. 26, no. 5, pp. 868–880, May 2016.
- [46] S. G. Chang, B. Yu, and M. Vetterli, "Adaptive wavelet thresholding for image denoising and compression," *IEEE Trans. Image Process.*, vol. 9, no. 9, pp. 1532–1546, Sep. 2000.
- [47] S. W. Smith, *The Scientist & Engineer's Guide to Digital Signal Processing*. San Diego, CA, USA: California Technical Publication, 1997.
- [48] J. S. Yedidia, W. T. Freeman, and Y. Weiss, "Generalized belief propagation," in *Proc. NIPS*, vol. 13. 2000, pp. 689–695.
- [49] P. F. Felzenszwalb and D. P. Huttenlocher, "Efficient belief propagation for early vision," *Int. J. Comput. Vis.*, vol. 70, no. 1, pp. 41–54, Oct. 2006.



Mrinmoy Ghorai received the B. Sc. degree in mathematics and the M.Sc. degree in pure mathematics from the University of Calcutta, Kolkata, India, in 2003 and 2005, respectively, and the M.Tech. degree in computer science from the Indian Statistical Institute, Kolkata, India, in 2009. He is currently a Project Linked Personnel with the Indian Statistical Institute and also pursuing the Ph.D. degree with the Indian Institute of Engineering Science and Technology, Shibpur, Howrah, India. His research interests include image inpainting, image restoration, and event recognition.



Sekhar Mandal received the B.Tech and M.Tech. degrees from the University of Calcutta, India, and the Ph.D. degree from Bengal Engineering and Science University, Shibpur, Howrah, India. He is currently an Associate Professor with the Computer Science and Technology Department, Indian Institute of Engineering Science and Technology, Shibpur, Howrah, India. His research interest mainly lies in digital image processing and pattern recognition.



Bhabatosh Chanda received the B.E. degree in electronics and telecommunication engineering and the Ph.D. degree in electrical engineering from the University of Calcutta, Kolkata, India, in 1979 and 1988, respectively. He is currently a Professor with the Indian Statistical Institute, Kolkata, India. He received the Young Scientist Medal of the Indian National Science Academy in 1989, the Vikram Sarabhai Research Award in 2002, and the IETE-Ram Lal Wadhwa Gold Medal in 2007. He is a fellow of the Institute of Electronics and Telecommunication Engineers, the National Academy of Science, India, the Indian National Academy of Engineering, and the International Association of Pattern Recognition.